©2011 IEEE. Personal use of this material is permitted. Permission from IEEE must be obtained for all other uses, in any current or future media, including reprinting/republishing this material for advertising or promotional purposes, creating new collective works, for resale or redistribution to servers or lists, or reuse of any copyrighted component of this work in other works. OCEANS 2011 IEEE **DOI: 10.1109/Oceans-Spain.2011.6003386**

Optimal Trajectory Generation for Draped AUV Gravity Surveys

Jacob Izraelevitz - Franklin W. Olin College of Engineering*

***Abstract*—Gravity surveys provide crucial data about the subseafloor structure, and this information is used to both localize and characterize geophysical phenomena. Obtaining this gravity data from submersibles provides superior measurements, both in terms of signal strength and spatial resolution, than conventional survey platforms such as surface vessels and satellites. However, performing gravimetry an AUV requires specialized trajectory planning algorithms that minimize acceleration noise. We develop an AUV simulation as a testbed for creating these algorithms, designed to model the behavior of the *Sentry* AUV at the Woods Hole Oceanographic Institution. We then investigate the signal and noise characteristics of AUV gravimetry and propose a novel trajectory planner and state estimator that mitigates multiple noise sources. The resulting simulation predicts a .22mGal standard deviation of signal noise, at a spatial resolution of 10m, for a magma chamber with a 3.41 mGal gravity signature at depth, substantially better than other tested draped surveying techniques.**

***Index Terms*—AUV, gravimetry, control**

I. Introduction

THE the study of variations in Earth's gravity field has a long history in military, private industry, and scientific institutions. Oil reservoirs, hydrothermal vent fluid, and mineral deposits all leave small detectable gravity signatures, and global maps of gravity variations are important for missile control. Ship gravimeters have been deployed since the mid 20th century for measuring seafloor gravity fluctuations.

Decreasing the sensor's distance to any gravity anomaly substantially increases the signal strength. Therefore, if the signal is too small to measure from ship-based gravimeters, the gravity sensor must be submerged, adding substantial technical challenges. However, to date, submerged gravimetry has been achieved on a moving platform with ROVs or manned submersibles (e.g., [8], [3], [11]) or underway from from towsleds or manned submersibles (e.g., [2], [16]).

AUVs (Autonomous Underwater Vehicles) are a logistically promising alternative to these survey methods. Already, autonomous vehicles have proved substantially cheaper to operate for other sensing tasks, such as magnetic and chemical sensing, because an AUV can perform multiple-hour surveys while the ship performs other functions. AUV-based gravity surveys have the potential to improve our ability to obtain gravity measurements at a reduced cost compared to previously reported ROV or manned submersible surveys.

*Undergraduate senior at Franklin W. Olin College of Engineering. Research performed under the Summer Student Fellowship program at Woods Hole Oceanographic Institution, supervised by Dr. James Kinsey.

Expanding gravimetry into the AUV sensing suite requires the development of new control techniques because an AUV, being untethered and autonomous, has to control its own trajectory with high fidelity to obtain accurate gravity measurements. This paper investigates the signal and noise characteristics of AUV gravimetry, proposes a trajectory generator and state estimator for an AUV, and compares the proposed trajectory generator with traditional AUV surveying techniques. These algorithms are tested in a simulated gravity survey of a typical magma chamber 700m below the seafloor [15].

II. Geophysical Motivation

Gravimetry surveys on a 1-10 mGal scale (1mGal=10^{-5}m/s^2) can detect and characterize a wide variety of geophysical phenomena. The Earth's gravitational field is not uniform; rather, it contains slight variations from a number of sources including the density distribution of mass within the crust and topological features [9]. The signal itself follows the familiar Newton's law of gravitation. Given a test mass m and large point mass M separated by distance r (Figure 1), the force on the test mass can be determined by the inverse square law [10]:

$$F_g = \frac{GmM}{r^2} \tag{1}$$

where G is the universal constant of gravitation. If we measure the force on a known test mass with a high resolution force meter, the mass and depth of small density variations can be detected with enough contrast to resolve variations in the density of the Earth's crust. A map of the gravity field, especially once combined with magnetic and bathymetric data, can then be fit to a model of rock type and distribution. This surveying technique has been used in a wide variety of applications in scientific investigations and in commercial applications such as petroleum and mineral exploration.

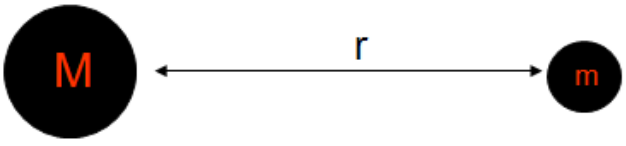

Figure 1. *Newton's Law of Gravitation* - The force measured by a gravimeter is proportional to the inverse square of the distance to the gravity anomaly.

Accurately measuring gravity from a moving platform requires an inertial reference frame or accurate knowledge of the vehicle's acceleration, because the vehicle's acceleration

is also measured by the gravimeter. For example, a gravimeter in free fall will not register any signal. Some gravimetric measurement techniques completely avoid this problem by having a fixed platform, such as stationary seafloor gravimeters for monitoring oil reservoir capacity. Unfortunately, using many such devices in a large seafloor survey is cost prohibitive.

Mobile gravity surveying platforms can correct for this error by measuring the platform's acceleration with some other non-inertial sensor. In AUV gravimetry, this vertical acceleration can be determined by taking the second time derivative of the depth sensor data. Therefore, to resolve the gravity anomaly, the vertical vehicle acceleration (VIGA - vehicle induced gravimeter acceleration) must be subtracted from the raw gravimeter measurement [2]:

$$g_{true} = g_{measured} - VIGA \tag{2}$$

The VIGA is a function of the vertical vehicle acceleration $\ddot{z}$, as well as any angular corrections from the pitch and roll ($\theta$and ψ) if the gravimeter is not coincident with the center of motion of the vehicle [4].

$$VIGA = \dot{J}_1\dot{\theta} + \dot{J}_2\dot{\psi} + J_1\ddot{\theta} + J_2\ddot{\psi} + \ddot{z} \tag{3}$$

A full derivation of the gravity anomaly parsing method, including definitions for the functions J_1, J_2, $\dot{J}_1$, $\dot{J}_2$, is available in the appendix of [4].

Error in this correction, either from the vertical acceleration or pitch and roll terms, adds noise to the corrected gravimeter measurement beyond the natural sensor noise in the gravimeter. Typically, this noisy signal must be heavily low-pass filtered to provide useful information. Unfortunately, low-pass filtering a signal will average the signal value in time, and because the platform is moving, this time-averaging will degrade the spatial resolution of the final gravity anomaly.

Depending on how aggressively the signal is filtered, the geologist can tradeoff signal amplitude resolution for spatial resolution and vice versa. This tradeoff can be optimized for the predicted characteristics of a gravity anomaly of interest. Figure 2 enumerates some gravity anomalies of geologic interest and their relative ease of measurement. For example, a mantle process has a spatially large but low amplitude gravity signature, meaning it can be detected by averaging over a wide filter window. Getting closer to the anomaly can be used to improve the spatial resolution or signal amplitude, or both, increasing the set of detectable anomalies.

A developed example of a practical application of near-bottom gravimetry is given in [6], and is reproduced here with permission. Fine-spatial resolution gravity data in MOR crustal terrains could be used to better understand crustal structure for the Main Endeavor hydrothermal vent Field (MEF) located on the Juan de Fuca Ridge. Multibeam bathymetric sonar and three-axis magnetometer surveys provide an intriguing view of how sub-seafloor structure at this site has been impacted by hydrothermal fluid flow (Figure 3). The Bastille and Dante-Grotto vents are separated by 200m and the magnetic data suggests independent upflow zones beneath the two vent systems [14]. High-resolution magnetic surveys provide only a partial picture of the sub-seafloor structure. Augmenting

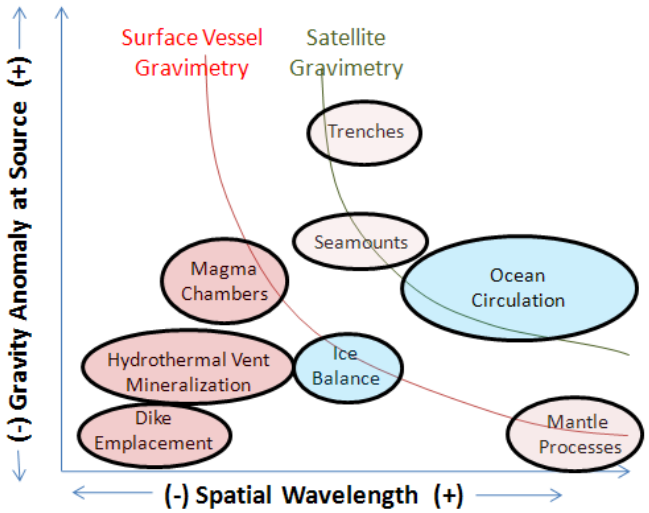

Figure 2. *Detectability of Gravity Anomalies* - Depending on the target anomaly, the gravity signal can be filtered to optimize for signal amplitude or spatial resolution, illustrated by the curves. Getting physically closer to the anomaly, such as moving from satellite to ship gravimetry, improves both signal amplitude and spatial resolution, allowing smaller anomalies to be detected. The geologic phenomena below the red line, such as hydrothermal vents and dikes, are currently very difficult to detect without resorting to near-bottom gravity measurements.

these magnetic measurements with near-bottom gravity data of comparable spatial resolution would significantly advance our ability to define the geometry and depth extent of these processes.

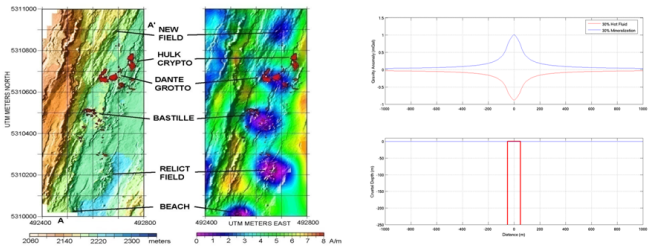

Figure 3. *Bathymetry, Magnetics, and Postulated Gravity at MEF* - Left panel shows seafloor micro-bathymetry of the MEF with red areas showing the main vent locations. Right panel shows crustal-magnetization — note the correlation of circular magnetization lows with active and inactive vent areas (from [14]).

For example, we modeled two cases for a hypothetical gravity survey of the MEF. We assumed a vertical cylinder of 50m radius, extending to infinite depth, measured at an altitude of 20m. The first case assumes that the crust contained within the cylinder is partially impacted by $350°C$ hydrothermal vent fluid, resulting in a negative density contrast between the impacted and surrounding crust. This contrast results in gravity reduction on the order of 1mGal (red line, Figure 2, top plot). The second case assumes that metal sulfide precipitation is occurring within the cylinder contained crust, resulting in a positive density contrast and producing a gravity increase on the order of 1mGal (blue line, Figure 2, top plot). This simple model underscores how near bottom gravimetry, along with other remote-sensing techniques, can provide a

more comprehensive picture of the subsurface structure of hydrothermal upflow zones.

III. Signal Strength and Noise Characteristics

The signal strength and noise characteristics of gravity surveys provide a basis for AUV survey design. The origins of these quantities are discussed in the sections below.

A. Signal Strength Characteristics

For a given trajectory, the signal strength of the anomaly can be derived directly from Newton's Law of Gravitation. If we assume the anomaly is a point mass M some at some location $[x_a, y_a, z_a]$, the signal power is:

$$P_{grav} = (GM/d^2)^2 \tag{4}$$

where:

$$d = \sqrt{(x - x_a)^2 + (y - y_a)^2 + (z - z_a)^2}$$

However, if we assume no prior knowledge of the horizontal location of the anomaly, but only its approximate depth, then the distance term simplifies to:

$$d = a + mbsf \tag{5}$$

where $mbsf$ (meters below seafloor) is the expected depth of the anomaly below the seafloor, and a is the vehicle's altitude above the seafloor. Rough knowledge of the $mbsf$ parameter is key to AUV gravity survey design, because it gives the tradeoff for signal strength as a function of survey altitude. While the exact depth of the geophysical features is rarely known in advance, the type of feature being investigated can inform this parameter. For example, a dike will typically have a $mbsf$ value on the order of 1-100m; a magma chamber will be deeper with a depth often greater than 1000m.

While we employ a point-mass model in the reported simulation, other models which integrate density over a volume (e.g. those discussed in [1]) could also be employed.

B. Noise Characteristics

There are several sources of gravimetry noise, broadly divided into path dependent and path independent. The AUV trajectory should be designed to minimize path dependent noise, while path independent noise must be reduced by other techniques.

1) Path Dependent Noise Sources: The path dependent noise comes from resolving the vertical acceleration (VIGA) signal of the vehicle. This vertical acceleration is measured by taking the second time derivative of the depth sensor data. Taking the derivative of a signal will generally increase noise, however, even an ideal noiseless sensor will have path dependent noise purely from numerical error.

The second derivative of signal $z(t)$ measured at discrete points spaced by Δt is given by:

$$\ddot{z}(t) = \frac{z(t + \Delta t) - 2z(t) + z(t - \Delta t)}{\Delta t^2} + O(z^{(4)}, \Delta t^2) \tag{6}$$

where the error O in this calculation is on the order of $z^{(4)}$ and Δt^2. Involving more than three points in the derivative calculation will decrease the error. For example, the five point stencil for taking a second derivative has error on the order of $z^{(6)}$ and Δt^4 (Equation 7). This method of taking derivatives, as well as arbitrarily larger stencils, can be derived from a Taylor series centered at t.

Regardless of the method for numerically taking a second derivative, the error in this calculation will be increased by a high amplitude in the higher derivatives of the vehicle path. In essence, high frequency components of the vehicle acceleration will add noise derived from numerical error.

A small time delay between the the acceleration measurement and the gravimeter measurement causes additional noise. The final corrected gravity anomaly, ignoring angular terms, is given by the difference between the measured acceleration from the depth sensor and the gravity sensor (Equation 2). However, if the two sensors are not synced, the small time difference will add error ϵ equal to the change in vehicle acceleration $\ddot{z}$ over the timeshift Δt:

$$\epsilon = \ddot{z}(t + \Delta t) - \ddot{z}(t) = z^{(3)}(t)\Delta t \tag{8}$$

An ideal AUV trajectory should therefore also avoid rapid changes in acceleration, especially discontinuities, to avoid both numerical differentiation error and time-delay induced error.

2) Path Independent Noise: Sensors, specifically depth sensors and gravimeters, can be assumed to have noise amplitude independent of the sensor state. For example, the accuracy of a depth sensor is roughly constant within its depth range. This fact allows us to decouple the sensor noise sources from the path dependent noise sources. Path independent sensor noise has two effects: additive measurement noise on the gravity anomaly and navigation noise.

The most direct effect of this sensor noise is a purely additive noise component on the final anomaly measurement. The acceleration measured by the depth sensor is especially noisy because it involves the second derivative of a signal, which always amplifies high frequency noise. This noise source exists even if the AUV happens to be perfectly motionless, so the only means of attenuating this path independent sensing noise are low pass filtering techniques, which effectively average the signal over time. Ideally, other sources of noise would be eliminated to allow for as high of a cutoff frequency as possible on this filter, enhancing the spatial resolution of the gravimetry survey.

Navigation noise has a more subtle effect on the total gravimetry noise; it adds error in a similar fashion as a variable setpoint. If the vehicle controller believes it is slightly below the setpoint due to this navigation noise, it will try to compensate by accelerating the vehicle upwards, adding high frequency components to the acceleration signal that are later lost when taking the derivative numerically. However, a realtime state estimator (e.g. [7]) can strongly attenuate the noise. A state estimator, such as the Kalman filter, estimates the location and velocity of the vehicle by combining sensor measurements with a predictive model.

$$\ddot{z}(t) = \frac{-z(t+2\Delta t) + 16z(t+\Delta t) - 30z(t) + 16z(t-\Delta t) - z(t-2\Delta t)}{12\Delta t^2} + O(z^{(6)}, \Delta t^4) \tag{7}$$

In summary, an ideal AUV gravity sensing technique is to minimize acceleration changes, use a state estimator to mitigate acceleration noise, and then filter the final signal to obtain the intended spatial resolution.

IV. Methodology

Performing near-seafloor gravimetry from an AUV requires a trajectory planner that optimizes the signal and noise characteristics of the measured gravity anomaly. Trajectory planners are best developed on an actual AUV, however, given the monetary and time costs of operating deep ocean platforms, we built a vehicle modeling environment in simulation to test the planner.

The simulation consists of five parts shown in Figure 4: a trajectory planner, a state estimator, a controller, a vehicle model, and sensor models. These simulation components are described in Sections IV-A through IV-E. After simulation, the gravity anomaly is reduced from the data in post-processing. While it may be possible to resolve the gravity field in realtime, doing so adds computational load to the AUV and limits the range of possible filtering techniques.

A. Sensor Models

Several typical oceanographic sensors are required for taking gravimetry measurements. For simulation simplicity, all sensors are assumed to be calibrated to run at 10Hz.

Gravimeter: At present, a suitable gravimeter possessing the power and size requirements necessary for an AUV is not available. In preparation for this high resolution sensor, the model assumes a calibrated gravimeter with standard deviation of 0.1mGal.

Depth Sensor: Since the true acceleration of the vehicle must be subtracted from the gravimeter measurement, the vehicle must include a non-inertial method of measuring acceleration. Depth sensors have a long history in ocean science and are currently available at part-per-billion precision. The model assumes a calibrated *Paroscientific* depth sensor with standard deviation of 24ppb (parts per billion) of a 4000m range.

Doppler Velocity Log (DVL): Vertical accelerations can also be determined from velocities measured with a DVL, however, the error is much larger than a signal derived from the depth sensor. Therefore, the simulation only uses the DVL for obstacle avoidance and navigation instead of adding information to the gravimeter measurement. The model assumes a *Teledyne WHN 300*, with velocity error of 0.2cm/s plus 0.4% of the velocity, and 2cm of altitude error.

Photonic Inertial Navigation System: Computing the gravimeter anomaly requires angular correction terms provided by the PhINS. The model assumes a *IXSEA PHINS 6000* with angular accuracy of 0.01 degrees and 0.001 degrees/s. While the PhINS also measures accelerations, this measurement uses inertial methods and therefore also includes gravitational acceleration. Consequently, the PhINS cannot be used to correct the gravimeter for vehicle acceleration; in fact, if the PhINS acceleration was accurate to the mGal scale, it would be a gravimeter.

An extended discussion of navigation sensors and their advantages/disadvantages is presented in [5].

B. Controller Model

The controller model consists of a simple PD acceleration controller. The response is a function of the depth setpoint provided by the trajectory generator, the measured depth, and the measured velocity. The controller response is given by:

$$\tau = C_1(z_{goal} - z_{measured}) + C_2\dot{z}_{measured} \tag{9}$$

where $C_1$and $C_2$are tuned controller parameters, z_{goal} is the intended vehicle depth, and $z_{measured}$ and $\dot{z}_{measured}$ are the measured depth and vertical velocity. This control algorithm is equivalent to a damped oscillator moving toward a variable equilibrium point. While this controller model is a highly simplified version of the complex problem faced by vehicle controllers, it is similar enough to a true AUV depth controller to provide a first pass scenario. Optimizing the controller for AUV gravimetry was not considered in this study, but many of the noise characteristics explored are relevant to controller design.

C. Vehicle Model

Dynamic modeling of submersibles, especially AUVs, is a difficult task and an active area of research. For the purposes of exposition, we employ a dynamic model developed for ROVs [13] that has been employed for ROV vehicle control [12] and state estimators [7]. While the fidelity of this model is low when compared to the intended platform, the Woods Hole AUV *Sentry*, this model possesses the key characteristics of a body moving in water:

$$\ddot{z} = \alpha|\dot{z}|\dot{z} + \beta\dot{z} + \gamma + \tau \tag{10}$$

The model includes nonlinear damping $\alpha|\dot{z}|\dot{z}$, linear damping $\beta\dot{z}$, net buoyancy γ, and the force from the controller τ. The coefficients α, β, and γ were identified through parameter identification experiments similar to those reported in [13], and are normalized by vehicle and added mass (Table I).

Sentry has the ability to perform highly complex translational maneuvers to avoid obstacles by controlling its fluid control surfaces in addition to thruster torques. However, these maneuvers are expected to add substantial noise to the gravimetry measurement, so they should be avoided. In the absence of these maneuvers, we can assume the horizontal velocity of the vehicle remains roughly constant over a survey track, limiting our control problem to a single dimension in the vertical direction.

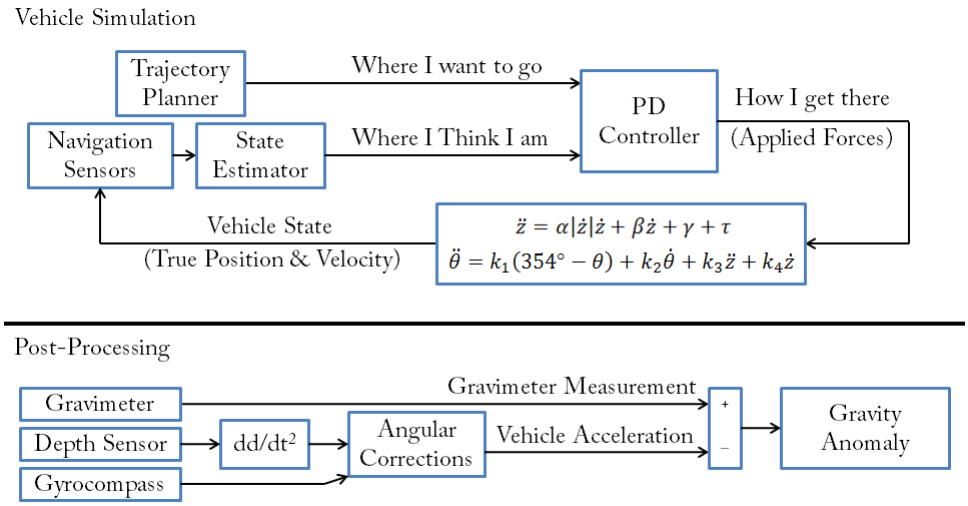

Figure 4. *System Flow Overview* - We focused our efforts on optimizing the trajectory planner and state estimator (top left) for a high quality gravity survey (bottom right) using a simulated vehicle. The code base includes two parts, a vehicle simulation and post-processing. The simulation numerically integrates the vehicle motion using a trajectory generator, a controller, a theoretical vehicle model, and sensor models. Post simulation, the gravity anomaly is derived and filtered from logged sensor data.

The gravity measurement is also sensitive to the pitching of the vehicle over a trackline; unfortunately, it is substantially more difficult to develop a fluids-based model of vehicle pitch. A simple curve fit based on vehicle measurements was instead used.

$$\ddot{\theta} = k_1(\theta - \theta_{eq}) + k_2\dot{\theta} + k_3\ddot{z} + k_4\dot{z} \tag{11}$$

This model consists of a restoring torque to the upright position of the vehicle $k_1(\theta - \theta_{eq})$, a damping torque $k_2\dot{\theta}$, and two torques proportional to the vertical acceleration and vertical velocity of the vehicle $k_3\ddot{z} + k_4\dot{z}$ (Table I). These torques are normalized by the vehicle's moment of inertia.

Table I
VEHICLE MODEL PARAMETERS

Parameter	Symbol	Value
Nonlinear Drag	α	$-.6118\ m^{-1}$
Linear Drag	β	$-.1532\ s^{-1}$
Net Buoyancy	γ	$-2.175 \times 10^{-3}\ m/s^2$
Equilibrium Pitch	θ_{eq}	$354°$
Righting Moment	k_1	$-1s^{-2}$
Damping Moment	k_2	$-2s^{-1}$
Acceleration Moment	k_3	$-50°/m$
Velocity Moment	k_4	$3°/m \times s$

D. State Estimator

The state estimator's purpose in the AUV survey is to mitigate navigation noise (Section III-B2) that adds high frequency oscillation into the acceleration correction. The state estimator augments the navigation sensors on the vehicle by integrating the sensors with a vehicle model.

The vehicle model is the same as the model given in Equation 10, however, instead of written as a single second-order differential equation, we split it into two first-order differential equations using the dummy variable v instead of $\dot{z}$. Also, the parameters α, β, and γ are varied by 10% to account for the vehicle's imperfect knowledge of its own parameters, giving new parameters α', β', and γ'. The system model is presented below:

$$\dot{z} = v \tag{12}$$

$$\dot{v} = \alpha'|\dot{z}|\dot{z} + \beta'\dot{z} + \gamma' + \tau \tag{13}$$

The state estimator consists of this imperfect vehicle model in addition to sensor input z_{meas} and v_{meas}, given by the depth sensor and DVL respectively. This sensory information is integrated into the two estimated quantities z_{est} and v_{est} using two gains L_1 and L_2:

$$\dot{z}_{est} = v_{est} + L_1(z_{meas} - z_{est}) \tag{14}$$

$$\dot{v}_{est} = \alpha'|\dot{z}_{est}|\dot{z}_{est} + \beta'\dot{z}_{est} + \gamma' + \tau + L_2(v_{meas} - v_{est}) \tag{15}$$

The resulting system of Equations 14 & 15, run with simulated sensor and trajectory data, gives a smooth estimation of vehicle state to the controller. The controller then applies forces to the vehicle with less high-frequency content, improving the final gravity signal.

E. Trajectory Generator

The trajectory generator gives the controller a depth setpoint as a function of time. Each of the following trajectory planners have a different signal and noise characteristics in the final gravity signal, and are therefore informative in constructing an optimized trajectory planner. Figure 5 illustrates simulated vehicle paths following these different trajectory generation techniques.

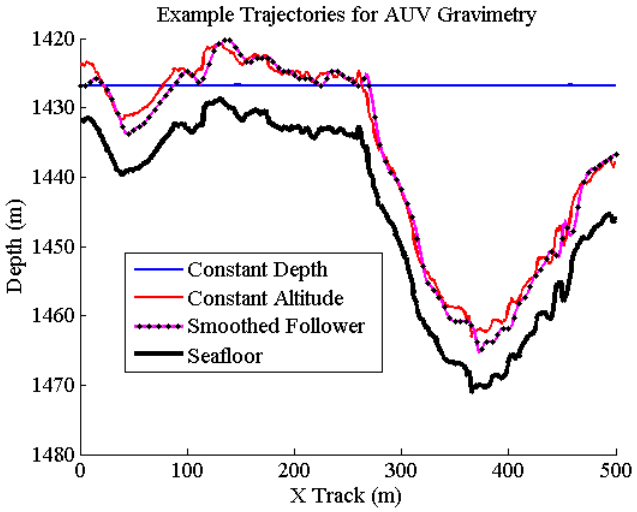

Figure 5. *Example Trajectories* - The constant depth survey maintains close to zero acceleration far from the seafloor, while the constant altitude and smoothed trajectory generator (Section V) follow the seafloor to obtain higher signal strength at the cost of higher vehicle acceleration and higher noise.

1) Constant Depth: A constant depth trajectory is the lower bound for noise power; the only noise sources are navigation and purely additive sensor noise (Section III-B2). Unfortunately, keeping a constant depth near the seafloor is dangerous with varying bathymetry, so a constant depth survey will have to be farther from the floor and therefore lose signal strength.

However, the rate at which the signal attenuates is dependent on the anomaly type, demonstrated by Equation 5. An anomaly deep under the seafloor (large predicted $mbsf$) will have a gravity signature relatively constant over small changes in altitude. For example, if the gravity anomaly is a magma chamber 2000m under the seafloor, a constant depth survey 50m above the seafloor only attenuates the signal strength by 5%.

2) Constant Altitude: If the anomaly is closer to the seafloor surface, hugging the terrain will provide a greater increase in signal. However, following the seafloor bathymetry at a fixed altitude will constantly accelerate and pitch the vehicle. Uncertainty in these quantities, caused by path dependent noise (Section III-B1), will create error in the VIGA correction, adding noise the final gravity measurement. The tradeoff is higher signal strength for higher noise.

Both these trajectory generation techniques are clearly suboptimal, but were tested in our simulation to demonstrate the different aspects of the problem and act as a comparison for our optimized trajectory design.

V. Smoothed Trajectory Generation

For the development of an ideal trajectory generator, we adopted the following criteria based on the signal/noise characteristics outlined in Section III and additional vehicle concerns:

- The trajectory generator should try to maintain constant stable regions with little numerical error, with transitions as smooth as possible between these states.
- The trajectory generator should adjust the noise allowance based on how strongly the signal attenuates with altitude. The limiting cases would therefore be a constant depth trajectory for signals with low altitude cost, and a smoothed constant altitude trajectory for signals with high altitude cost.
- The trajectory generator should maintain the vehicle within an altitude envelope.
- The trajectory generator should be predictive and run at a slower update rate than the controller, ideally around 0.1Hz.

A. Trajectory Smoothing

Given that the trajectory generator has to be piecewise if it is run only once every 10s, the largest noise source is likely the transition between trajectories. The following function, however, is both piecewise and smooth even at transition points:

$$f(x) = \begin{cases} 0 & if\ x \leq 0 \\ \frac{e^{-1/x}}{e^{-1/x}+e^{-1/(1-x)}} & if\ 1 < x < 0 \\ 1 & if\ x \geq 1 \end{cases} \quad (16)$$

If we numerically integrate the function to get $F(x)$, the resulting curve acts as a piecewise smooth transition between a slope of 0 and 1, instead of two values 0 and 1. Scaling the function then provides a smooth transition between two arbitrary vertical velocities v_i and v_f over an arbitrary timescale t_f (Figure 6):

$$t = t_f x + t_0 \quad (17)$$

$$z(t) = F(x)(v_f - v_i)t_f + v_i t_f x + z_0 \quad (18)$$

The proposed trajectory generator creates one of these profiles every iteration at 10-second intervals. Chaining these depth profiles together creates a piecewise depth setpoint function that maintains smooth transitions. This path function substantially decreases signal noise in comparison to the stepped depth and constant altitude algorithms (see Section VI).

B. Trajectory Selection

Every iteration of the trajectory generation has one degree of freedom, namely the final velocity at the end of the iteration. The final velocity is selected for high SNR (signal to noise ratio) and obstacle avoidance.

Evaluating the depth profile transform (Equation 17 & 18) at time t_f and then extrapolating along the final velocity gives a likely position of the vehicle some set time $t_{predict}$ in the future, usually on the order of 60 seconds for good vehicle performance:

$$z(t_{predict}) = \frac{1}{2}(v_f - v_i)t_f + v_i t_f + v_f(t_{predict} - t_f) + z_0 \quad (19)$$

Given bathymetric irregularity between t_0 and $t_{predict}$, the depth of the altitude envelope $[a_+,\ a_-]$ will possibly change

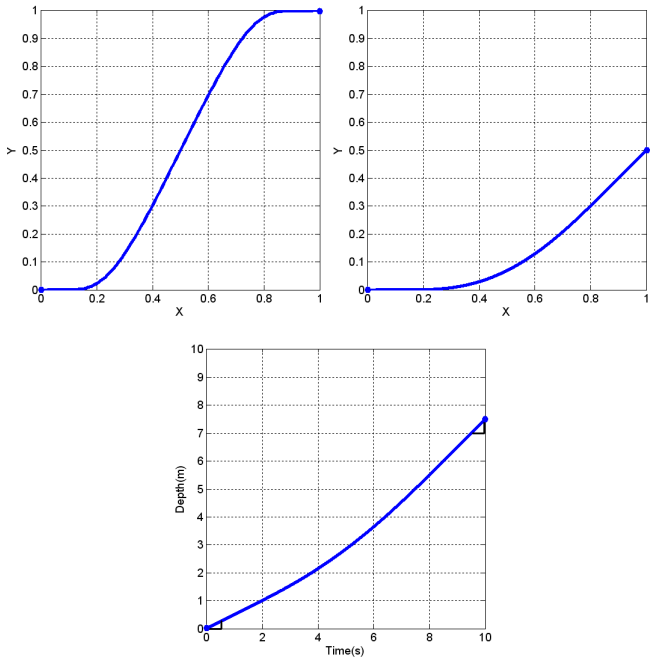

Figure 6. *Smooth Piecewise Trajectory* - A non-analytic smooth transition function from 0 to 1 (upper left) when integrated is a normalized trajectory that provides a smooth transition from a slope of 0 to a slope of 1 (upper right). After applying a scaling transform, the function is a smooth transition between two arbitrary vertical velocities (bottom center).

dramatically. This change can be predicted by logged DVL altitude measurements. If the DVL measured an altitude a at time t_{past} before the current time t, the forward-predicted envelope depth $[z_-, z_+]$ is given by:

$$[z_-, z_+] = z(t)+a(t)+(a(t)-a(t_{past}))\frac{t_{predict}}{(t-t_{past})}-[a_+,\ a_-] \tag{20}$$

where z is measured vehicle depth and a is measured vehicle altitude. This calculation assumes constant horizontal velocity.

After eliminating trajectories that do not fall within $[z_{shallower}, z_{deeper}]$ at time $t_{predict}$, the trajectory generator can choose the trajectory with the best expected signal to noise ratio. The SNR can be predicted using a model justified by the arguments listed in Section III:

$$SNR \approx \frac{(GM/d^2)^2}{n_{indep}+n_{path}(P)} \tag{21}$$

where n_{indep} and n_{path} are path independent noise constant and path dependent noise function, respectively, and P is the path vector. These can be derived analytically, but are easier instead to fit to simulation data. Our simulation used $n_{indep} = 6.5\times10^{-6}$ and $n_{path}(P) = 1.67\times10^{-9}(v_f - v_i)^2$, but these quantities are not universal and are instead a function of sensor and filter selection. Unfortunately, given the roughly three order of magnitude difference between n_{indep} and $n_{path}(P)$, the SNR gains from optimized path selection are small in comparison to path independent noise. The SNR gains from this algorithm instead come largely from the smooth setpoint transitions.

VI. Case Study: Magma Chamber

To test the described smooth trajectory generator, we prepared a simulated seafloor landscape with the gravity signature of a shallow magma chamber with seafloor bathymetry taken from logged *Sentry* data. We assumed the magma chamber consisted of a 600kg/m^3 density contrast sphere of radius 500m, located 700m below the seafloor. The observed gravity anomaly at seafloor was around 3.48mGal. In comparison to the example generators previously described, the smoothed trajectory generator consistently performed on par or better than the other techniques. Data from some sample runs is found in Table II.

Table II
Magma Chamber Simulation Results

Parameter	*Const. Depth*	*Const. Altitude*	*Smoothed*
Std. Deviation	.22mGal	.54mGal	**.22mGal**
Signal Mean	3.24mGal	3.41mGal	**3.41mGal**

For the magma chamber studied in this simulation, there is only a 5% signal strength increase for following the seafloor versus keeping a constant depth. A constant depth survey, with the state estimator included, is therefore a passable trajectory choice for flat seafloor terrain and gravity anomalies far below the seafloor. Other gravitational anomalies, such as hydrothermal vent mineralization, are nearer to the seafloor surface and often occur in more sloped terrain, so a smoothed trajectory generator would be a more attractive option. Regardless of the type of survey, a state estimator provides substantial gravity signal improvement. Navigation noise in the controller is such a large error source that a estimator decreases the signal noise by 80%, while the trajectory generator choice has a smaller effect on the final signal quality.

VII. Conclusions and Future Work

The potential benefits of AUV gravimetry will only be realized after significant sensor and algorithm development, however, the proposed trajectory framework provides a useful tool for enhancing that development. Gravimetric noise is due to multiple interdependent error sources that can be stymied by intelligent survey techniques:

- Numerical Error: Taking a second derivative discretely of a rapidly changing signal always includes numerical error. The rapid change can be caused by a fluctuating trajectory or a noisy navigation state, and must be solved by smoothed trajectory generation and navigation state estimation respectively.
- Measurement Noise: This sensor noise is purely additive, and must be low pass filtered.
- Navigation Noise: This sensing-based noise causes high frequency accelerations that later cause numerical error, and this noise best mitigated by state estimation prior to the controller.

The proposed trajectory smoothing algorithm shows substantial signal quality improvement over other bottom following techniques, while a constant depth survey shows promise for gravity anomalies with low signal attenuation over altitude

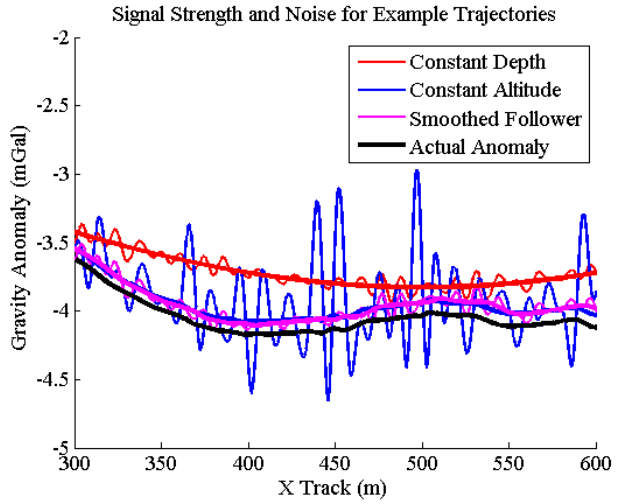

Figure 7. *Signal Characteristics* - The gravitational anomalies seen by the constant depth, constant altitude, and the reported smoothed trajectory generator are shown. The bold curves are the ideal noiseless signal on each trajectory type, while the maximum possible signal strength is shown by the gravity on the seafloor (black curve). The sinusoids show the final gravity signals, 5th order butterworth filtered to a spatial resolution of 10m. The gravity anomaly is negative because of the negative density contrast between the magma chamber and the surrounding rock. Note that the smooth trajectory generator has the signal strength of a constant altitude survey, but with the low noise of a constant depth survey.

changes. Navigation error is the largest noise source, and, through the use of the reported state estimator, this error source can be significantly reduced.

VIII. Acknowledgements

I would like to thank my advisor Dr. James Kinsey for his constant aid and feedback, without which this project would not have been possible.

References

[1] Robert J. Blakely. *Potential Theory in Gravity and Magnetic Applications*. Cambridge University Press, 1995.

[2] James R. Cochran, Daniel J. Fornari, Bernard J. Coakley, Randall Herr, and Maurice A. Tivey. Continous near-bottom gravity measurements made with a BGM-3 gravimeter in DSV Alvin on the East Pacific Rise near 9°31'N and 9°50' N. *Journal of Geophysical Research*, 104(B5):10,841 – 10,861, May 1999.

[3] R.L. Evans. A seafloor gravity profile across the tag hydrothermal mound. *Geophysical Research Letters*, 23(23):3447–3450, 1996.

[4] Maurice A. Tivey James C. Kinsey and Dana R. Yoerger. Toward high-spatial resolution gravity surveying of the mid-ocean ridges with autonomous underwater vehicles. *IEEE/MTS Oceans*, 2008.

[5] James C. Kinsey, Ryan M. Eustice, and Louis L. Whitcomb. A survey of underwater vehicle navigation: Recent advances and new challenges. In *IFAC Conference of Manoeuvering and Control of Marine Craft*, Lisbon, Portugal, September 2006. Invited paper.

[6] James C. Kinsey, Maurice A. Tivey, and Dana R. Yoerger. Toward high-spatial resolution gravity surveying of the mid-ocean ridges with autonomous underwater vehicles. Quebec City, Canada, September 2008.

[7] James C. Kinsey and Louis L. Whitcomb. Model-based observers for underwater vehicle navigation: Theory and preliminary experiments. pages 4251–4256, Rome, Italy, April 2007.

[8] B. P. Luyendyk. On-bottom gravity profile across the east pacific rise crest at 21ř north. *Geophysics*, 49(12):2166–2177, 1984.

[9] Jr. Nash, R.A. and S.K. Jordan. Statistical geodesy — an engineering perspective. *Proceedings of the IEEE*, 66(5):532–550, 1978.

[10] Issac Newton. *Mathematical Principles of Natural Philosophy*. 1687.

[11] Glenn S. Sasagawa, Wayne Crawford, Ola Eiken, Scott Nooner, Torkjell Stenvold, and Mark A. Zumberge. A new sea-floor gravimeter. *Geophysics*, 68(2):544–553, 2003.

[12] David A. Smallwood. *Advances in Dynamical Modeling and Control of Underwater Robotic Vehicles*. PhD thesis, The Johns Hopkins University, Baltimore, MD, USA, January 2003.

[13] David A. Smallwood and Louis L. Whitcomb. Adaptive identification of dynamically positioned underwater robotic vehicles. *IEEE Transactions on Control System Technology*, 11(4):505–515, 2003.

[14] M. A. Tivey and H.P. Johnson. Crustal magnetization reveals subsurface structure of juan de fuca ridge hydrothermal vent fields. *Geology*, 30(11):979–982, 2002.

[15] M. West, W. Menke, and M. Tolstoy. Focused magma supply at the intersection of the cobb hotspot and the juan de fuca ridge. *Geophysical Research Letters*, 30(14), 2003.

[16] M. A. Zumberge, J. R. Ridgway, and J. A. Hildebrand. A towed marine gravity meter for near-bottom surveys. *Geophysics*, 62(5):1386–1393, 1997.